PICOSECOND TIME RESOLUTION BY A CONTINUOUS WAVE LASER AMPLITUDE MODULATION TECHNIQUE III: DUAL-BEAM LUMINESCENCE EXPERIMENT

HEINRICH GUGGER and GION CALZAFERRI

Institute for Inorganic and Physical Chemistry, University of Bern, Freiestrasse 3, CH-3012 Bern (Switzerland)

(Received September 25, 1980; in revised form November 18, 1980)

Summary

A dual-beam luminescence experiment is presented which is designed to investigate very small changes, down to 20 ps, in radiative lifetimes in the nanosecond range. The diffusion-controlled mechanism of collisional luminescence quenching serves as an example to demonstrate under which conditions absolute photophysical data can be calculated on the basis of relative time measurements. Statistics are applied to verify the validity of the results.

The dual-beam method is well suited to check kinetic statements. Furthermore, it is a valuable proof for the reliability of the time resolution.

1. Introduction

1.1. Objective

Most spectroscopic techniques evolve from the single-beam principle to the double-beam version. Decisive reasons are the resolution enhancement and the removal of a series of accompanying inconveniences such as instrumental parameters and solvent contributions.

The ideal double-beam experiment links specific sample and reference information, carried by their individual beams, to a composite signal before detection takes place. Chopping techniques approach this case only if high time resolution is not required.

If time resolution becomes the point of interest, a need for the simultaneous acquisition of information on both channels arises. A possible solution is the use of two separate detection units. Here the problem of calibrating the system with respect to inequalities is encountered. If only a single detector is used, the beam information has to be structured in such a way that the interference pattern of the two beams transmits the information which is specific for the sample under study.

0047-2670/81/0000-0000/$02.50

In conventional set-ups real time applications with ultrashort pulses are better adapted to acquisition with two detectors. Otherwise some sort of multiplexing by means of optical delays should be performed.

Modulation techniques allow this information overlay where the basic structure consists of intensity modulation. The sample characteristic is the dephasing or the compression of the beam modulation. Birks and Munro [1] have carefully reviewed modulation fluorimetry. Neither in these nor in newer experiments has a double-beam principle been applied.

In the present work we introduce this feature and show that relative measurements do not necessarily cause a loss in the absolute parameters.

1.2. The chemical model

There are still many interesting questions to be answered in the fields of energy transfer processes and photoredox reactions and in studies of other possible relaxation channels of optically excited molecules (see for example ref. 2). Among these, luminescence quenching serves as a straightforward means of studying deactivation and is taken as a chemical model mechanism for this work. When a diffusion-controlled mechanism is assumed for collisional quenching (see for example ref. 3) at low dye concentrations (below 10^{-6} mol l^{-1}), the following steps must be considered.

$^1A^* \xrightarrow{k_F} {}^1A + h\nu$		emission
$^1A^* \xrightarrow{k_{ISC}} {}^3A^*$		intersystem crossing
$^1A^* \xrightarrow{k_t} {}^1A$		internal conversion
$Q + {}^1A^* \xrightarrow{k_q} {}^1A + Q$		quenching

The kinetic equation relating the fluorescence lifetime to the rate constants is

$$\tau_i = \frac{1}{k_F + k_{ISC} + k_t + k_q[Q_i]} \tag{1}$$

where $[Q_i]$ denotes the concentration of the quencher in moles per litre.

2. The dual-beam matrix method

The modulation measurement concept [4] as well as the experimental aspects of this technique [5] have already been fully described. We now present one of the applications.

A number n of dye solutions is prepared with different contents $[Q_i]$ (where $i = 1,...,n$) of quencher. This set is duplicated and, in a chess-board-like manner, every solution of concentration $[Q_i]$ is measured against every solution of concentration $[Q_j]$. The $[Q_i]$ solution is placed in the sample

housing and the $[Q_j]$ solution is placed in the reference housing (ref. 5, Fig. 1). The result of each determination is a lifetime difference τ_{ij}. According to eqn. (1) τ_{ij} can be written in the following form, where we substitute $k = k_{ISC} + k_F + k_t$ for convenience:

$$\tau_{ij} = \frac{1}{k + k_q [Q_i]} - \frac{1}{k + k_q [Q_j]} \tag{2}$$

The set of n solutions thus gives n^2 non-linear equations which allow the rate constants k and k_q to be determined.

2.1. Determination of the rate constants

Every measured lifetime difference τ_{ij} can be related to a theoretical time difference $t_{ij}(k, k_q)$ which is calculated according to eqn. (2). In making use of the n^2 measured values, the deviations from measured τ_{ij} and theoretical t_{ij} values have to be minimized with respect to the rate constants k and k_q. As outlined earlier [4] we attribute a gaussian distribution to the measurement errors. We therefore write

$$A(k, k_q) = \sum_i \sum_j \{t_{ij}(k, k_q) - \tau_{ij}\}^2 \tag{3}$$

The best fit of the rate constants to the measured times is achieved where A reaches a minimum, *i.e.* when $(\partial A/\partial k)_{k_q} = 0$ and $(\partial A/\partial k_q)_k = 0$. To obtain a criterion for the reliability of the fitted rate constants, standard statistical methods were applied. To make sure that, within the error of the data, a well-defined minimum exists, the topography of the three-dimensional hypersurface $A(k, k_q)$ was analysed (see Fig. 1).

At the minimum A^0 the standard deviation σ and the 95% confidence interval 4σ of A^0 can be calculated by applying parabolic interpolation without any loss of information [6].

No statistics are established for the errors in the quencher concentration $[Q_i]$. Numerical controls have shown that an error of 1% causes time shifts of below 5 ps, which lie well within the accuracy limit of $\Delta\tau_{ij} \approx 20$ - 30 ps.

2.2. Kinetic model test and accuracy proof

As a visualization of the fit we display the measured lifetime differences τ_{ij} in a chess-board scheme (Figs. 3 and 6). Instead of plotting τ_{ij} *versus* $[Q_i]$ and $[Q_j]$, which would lead to a curved surface, we transform the coordinates by analogy with the Stern–Volmer plot to obtain a plane. The coordinates to be used are t_i on the x axis and t_j on the y axis, where t_i and t_j denote the absolute radiative lifetimes of samples i and j respectively and are calculated from eqn. (1) using the fitted values for k and k_q.

The fitted plane can be written in analytical form as

$$t_{ij} = t_i - t_j$$

It becomes zero for $i = j$ and is antisymmetric with respect to $t_i = t_j$. The

TABLE 1

Concentration chart for the quencher KI[a]

Type I		*Type II*		*Type C*	
Code	c (mol l^{-1})	*Code*	c (mol l^{-1})	*Code*	c (mol l^{-1})
6	0	1	0.03960	1	0
1	0.01108	2	0.04291	2	0.02167
2	0.02306	3	0.04696	3	0.05239
3	0.03961	4	0.05040	4	0.09930
4	0.05844	5	0.05431	5	0.17977
5	0.08396	6	0.05844	6	0.35000

[a]The designation of types I, II and C is explained in the text (see Section 4).

goodness of the fit is checked by comparison of the experimental values τ_{ij} with the fitted values t_{ij}.

The accuracy of the modulation technique can be checked by applying two model independent criteria.

(1) The more closely the values for τ_{ii} approach zero, the more accurate is the method, because this may be considered as a calibration measurement at an exactly known theoretical value $t_{ii} = 0$ which is independent of [Q], k and k_q and hence of the model itself.

(2) The more completely the antisymmetry for $\tau_{ij} = -\tau_{ji}$ is satisfied, the higher is the probability that the measurement system is free from artefacts.

3. Experimental conditions

The dye Rhodamine B extra SP (BASF) was used without further purification in non-degassed solutions at concentrations below 10^{-6} mol l^{-1}. The solvent used was a mixture of 90% absolute ethanol (p.a. Merck) and 10% doubly distilled water. The quencher employed was neutral KI (p.a. Merck) at the concentrations given in Table 1.

The excitation wavelength was the 530.9 nm line of a krypton ion laser at power levels of some milliwatts. The emission bandwidth was selected using a Balzers interference filter centred at $\lambda = 588$ nm and with a full width at half-maximum of 42 nm. The modulation frequency was approximately 35 MHz.

Data reduction of the measurements was performed on a PDP 11/05 computer inherent to the Tektronix WP2221 acquisition system running under TEK SPS BASIC. The contour matrix was generated on an IBM 370 computer using FORTRAN IV with double precision and was plotted [7] using Tektronix graphic terminals.

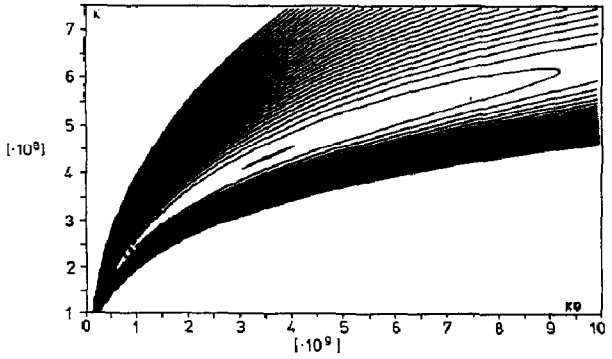

Fig. 1. An iso-error-square (IES) map for measurements of type I: the error topography for a wide span of rate constant coordinates. The distance between the equicontours is 250σ. The deepest line marks the 95% confidence level.

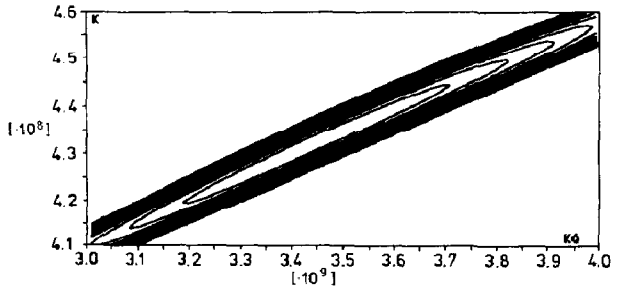

Fig. 2. An IES map for measurements of type I: the error topography in the proximity of the minimum. The distance between the equicontours is σ. The first trace locates σ above the minimum ($A^0 + \sigma$).

4. Results

The concentration range of the added quencher fixes the type of information to which there is ready access.

(1) The large range for type I information is appropriate for calculating the photophysical constants k and k_q.

(2) The small range for type II information serves as an accurate resolution test and/or proof.

(3) The extra-large range for type C information is introduced for comparative purposes to underline the tendency. It was calculated only.

The accuracy of the measured lifetime differences does not depend on the concentration range.

4.1. Type I: the broad quenching range

The topography of the contour line diagrams strongly resembles a steep and narrow valley on the flat bottom of which resides a shallow pool reflecting our 95% confidence area (Fig. 1). To highlight the conditions in the proximity of the minimum, the contour data were recalculated for a smaller section and the results are shown in Fig. 2.

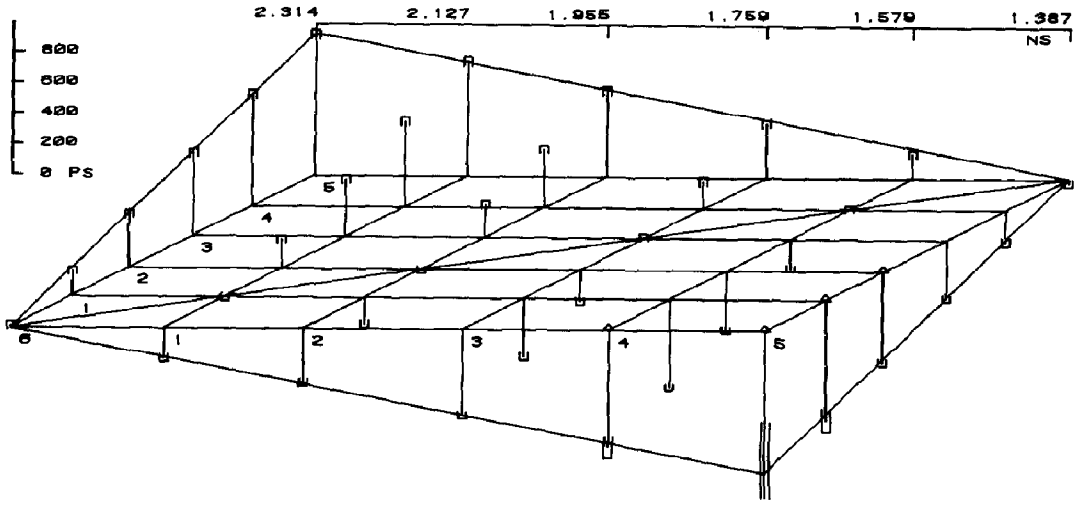

Fig. 3. A chess-board stick plot for type I measurements ($k = 4.32 \times 10^8\ s^{-1}$, $k_q = 3.44 \times 10^9\ l\ mol^{-1}\ s^{-1}$) (see text).

This procedure can be repeated many times and the appearance always remains the same. This reveals clearly that even if the valley is flat there is a definite minimum of reasonable structure. We consider this to be evidence for the kinetic model and at the same time as proof that the calculation is sufficiently precise to exclude numerical artefacts. The fitted rate constants hence evaluate to

$$k = (4.32 \pm 0.3) \times 10^8\ s^{-1}$$

and

$$k_q = (3.44 \pm 0.5) \times 10^9\ l\ mol^{-1}\ s^{-1}$$

The uncertainty interval is given by the extrema of the 95% confidence surface with respect to the rate constant coordinates. Insertion of k and k_q into eqn. (2) allows the time domain plot of Fig. 3 to be set up.

In this figure every vertical stick denotes a measurement of τ_{ij}. The hats on top of the sticks represent the error intervals $\Delta\tau_{ij}$ resulting from the on-line error estimation described extensively in ref. 4. The measurements shown in Fig. 3 which are flagged with a triangle at the bottom of the stick were eliminated before the determination of the rate constants. They exceeded the dynamic range of our instrumental set-up and could only be acquired by means of a coarse disadjustment of the beam intensities. This obviously led to less accurate results. An impression of the accuracy achieved is given in Fig. 4.

There is a good correspondence between the error estimation and the effective deviations. It can be seen from Table 2 and Fig. 4 that the estimates were made cautiously as the real deviations from theory are about a factor of 2 smaller.

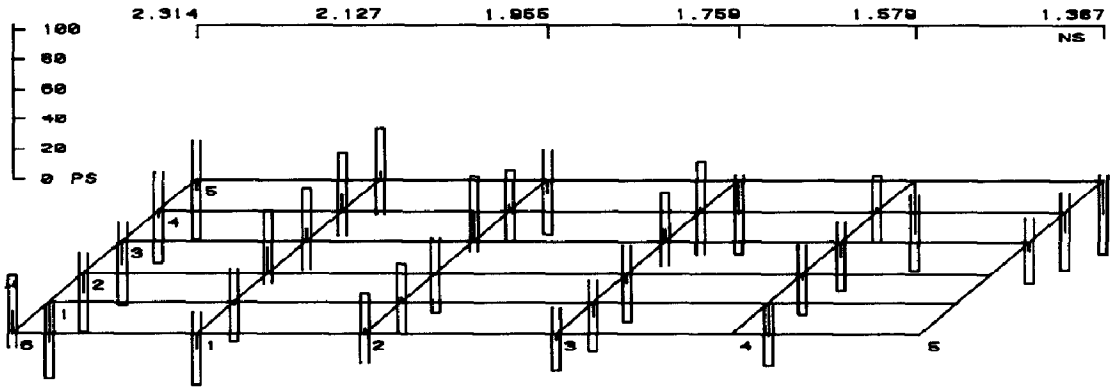

Fig. 4. The residues of Fig. 3 ($k = 4.32 \times 10^8$ s^{-1}, $k_q = 3.44 \times 10^9$ l mol^{-1} s^{-1}). The amounts $t_{ij} - \tau_{ij}$ (sticks) are shown in relation to the error intervals $\Delta\tau_{ij}$ (hats).

4.2. Type II: the small quenching range

A map analogous to that shown in Fig. 1 is plotted in Fig. 5. It is obviously no longer possible to minimize the rate constants in a reasonable way. The topography is much less steep over the whole region; therefore the experimental errors may change the structure of our valley significantly. Nevertheless our pool contains the (k, k_q) coordinates deduced for type I measurements. Using these constants we can build the time domain graph shown in Fig. 6, which reflects the high time resolution of the picosecond apparatus.

To emphasize the accuracy, auxiliary lines are added to Fig. 7. Their crossing points represent the theoretical times t_{ij}. The auxiliary plane thus formed corresponds to the plane shown in Fig. 4.

4.3. Model calculations

Three questions induced us to carry out such calculations.

(1) To what extent do the experimental errors distort the structure of the minimum?

(2) Which time resolution is required for this type of measurement to improve precision of the rate constants significantly?

(3) How does the structure of the IES map alter with increasing concentration span of the quencher?

The procedure for these investigations is essentially equivalent to that used to calculate the contour matrix. The only difference is that the errors $t_{ij} - \tau_{ij}$ are randomly generated and are normalized to a preset sum of error squares A^0. A matrix of theoretical time differences t_{ij} is set up according to eqn. (2) based on the fitted rate constants k and k_q of the appropriate case. Experimental data are then simulated by overlaying the random error distribution to the theoretical times.

TABLE 2

Data table for measurements of type I

Valid[a]	τ_{ij}[b] (s)	$\Delta\tau_{ij}$[c] (s)	t_{ij}[d] (s)	$t_{ij} - \tau_{ij}$ (s)	$[Q_i]$[e] (mol l^{-1})	$[Q_j]$[e] (mol l^{-1})
1	-2.19632×10^{-12}	2.40818×10^{-11}	0.0	2.19632×10^{-12}	0.01108	0.01108
1	1.89206×10^{-10}	2.44690×10^{-11}	1.71448×10^{-10}	-1.77582×10^{-11}	0.01108	0.02306
1	3.75526×10^{-10}	2.72341×10^{-11}	3.67390×10^{-10}	-8.13611×10^{-12}	0.01108	0.03961
1	5.58968×10^{-10}	2.76822×10^{-11}	5.47462×10^{-10}	-1.15056×10^{-11}	0.01108	0.05844
1	7.45081×10^{-10}	2.89249×10^{-11}	7.39856×10^{-10}	-5.22479×10^{-12}	0.01108	0.08396
1	-1.97717×10^{-10}	2.42824×10^{-11}	-1.87687×10^{-10}	1.00304×10^{-11}	0.01108	0.00000
1	-1.68437×10^{-10}	2.29980×10^{-11}	-1.71448×10^{-10}	-3.01085×10^{-12}	0.02306	0.01108
1	-8.61343×10^{-13}	2.50716×10^{-11}	0.0	8.61343×10^{-13}	0.02306	0.02306
1	2.14653×10^{-10}	2.52997×10^{-11}	1.95942×10^{-10}	-1.87110×10^{-11}	0.02306	0.03961
1	3.80572×10^{-10}	2.35763×10^{-11}	3.76015×10^{-10}	-4.55749×10^{-12}	0.02306	0.05844
1	5.59733×10^{-10}	2.82386×10^{-11}	5.68408×10^{-10}	8.67536×10^{-12}	0.02306	0.08396
1	-3.55399×10^{-10}	2.32014×10^{-11}	-3.59134×10^{-10}	-3.73549×10^{-12}	0.02306	0.00000
1	-3.76387×10^{-10}	2.37921×10^{-11}	-3.67390×10^{-10}	8.99711×10^{-12}	0.03961	0.01108
1	-2.02020×10^{-10}	2.54323×10^{-11}	-1.95942×10^{-10}	6.07795×10^{-12}	0.03961	0.02306
1	8.32948×10^{-12}	2.41338×10^{-11}	0.0	-8.32948×10^{-12}	0.03961	0.03961
1	1.82842×10^{-10}	3.09524×10^{-11}	1.80072×10^{-10}	-2.76953×10^{-12}	0.03961	0.05844
1	3.49461×10^{-10}	2.65514×10^{-11}	3.72466×10^{-10}	2.30053×10^{-11}	0.03961	0.08396
1	-5.58563×10^{-10}	2.08523×10^{-11}	-5.55077×10^{-10}	3.48647×10^{-12}	0.03961	0.00000
1	-5.69590×10^{-10}	2.01983×10^{-11}	-5.47462×10^{-10}	2.21276×10^{-11}	0.05844	0.01108
1	-3.79718×10^{-10}	2.32967×10^{-11}	-3.76015×10^{-10}	3.70349×10^{-12}	0.05844	0.02306
1	-1.89855×10^{-10}	2.27977×10^{-11}	-1.80072×10^{-10}	9.78253×10^{-12}	0.05844	0.03961
1	2.71816×10^{-12}	2.19482×10^{-11}	0.0	-2.71816×10^{-12}	0.05844	0.05844
1	1.56668×10^{-10}	2.52007×10^{-11}	1.92394×10^{-10}	3.57259×10^{-11}	0.05844	0.08396
0	-7.65723×10^{-10}	6.80048×10^{-11}	0.0	0.0	0.05844	0.00000
0	-7.80528×10^{-10}	7.59827×10^{-11}	0.0	0.0	0.08396	0.01108
0	-5.86105×10^{-10}	2.40757×10^{-11}	0.0	0.0	0.08396	0.02306
1	-3.78436×10^{-10}	2.19939×10^{-11}	-3.72466×10^{-10}	5.96968×10^{-12}	0.08396	0.03961
1	-2.05336×10^{-10}	2.59463×10^{-11}	-1.92394×10^{-10}	1.29421×10^{-11}	0.08396	0.05844
1	-2.27180×10^{-11}	2.65992×10^{-11}	0.0	2.27180×10^{-11}	0.08396	0.08396
0	-1.07982×10^{-9}	4.88707×10^{-10}	0.0	0.0	0.08396	0.00000
1	1.61331×10^{-10}	2.45032×10^{-11}	1.87687×10^{-10}	2.63556×10^{-11}	0.00000	0.01108
1	3.46481×10^{-10}	2.64577×10^{-11}	3.59134×10^{-10}	1.26535×10^{-11}	0.00000	0.02306
1	5.39586×10^{-10}	2.76218×10^{-11}	5.55077×10^{-10}	1.54905×10^{-11}	0.00000	0.03961
1	7.30671×10^{-10}	3.05440×10^{-11}	7.35149×10^{-10}	4.47800×10^{-12}	0.00000	0.05844
1	9.20285×10^{-10}	3.32186×10^{-11}	9.27543×10^{-10}	7.25785×10^{-12}	0.00000	0.08396
1	1.47279×10^{-11}	2.38942×10^{-11}	0.0	-1.47279×10^{-11}	0.00000	0.00000

[a] The number of valid measurements (valid = 1) is 32; measurements with valid = 0 correspond to the flagged measurements in Fig. 3.

[b] τ_{ij} is the measured lifetime difference.

[c] $\Delta\tau_{ij}$ is the calculated error of τ_{ij} (see ref. 4).

[d] t_{ij} is the calculated time for optimum k and k_q.

[e] [Q] is the quencher concentration.

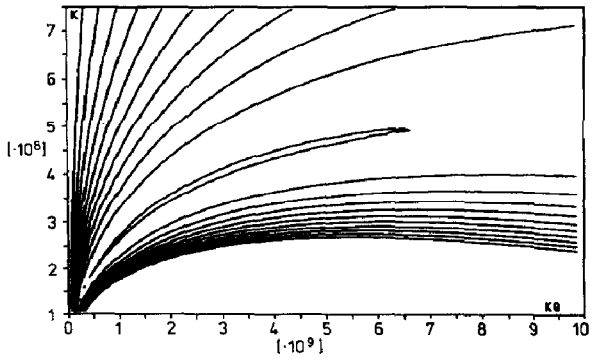

Fig. 5. An IES map for measurements of type II: the error topography for a wide coordinate span. The distance between the equicontours is 250σ. The deepest line marks the 95% confidence level.

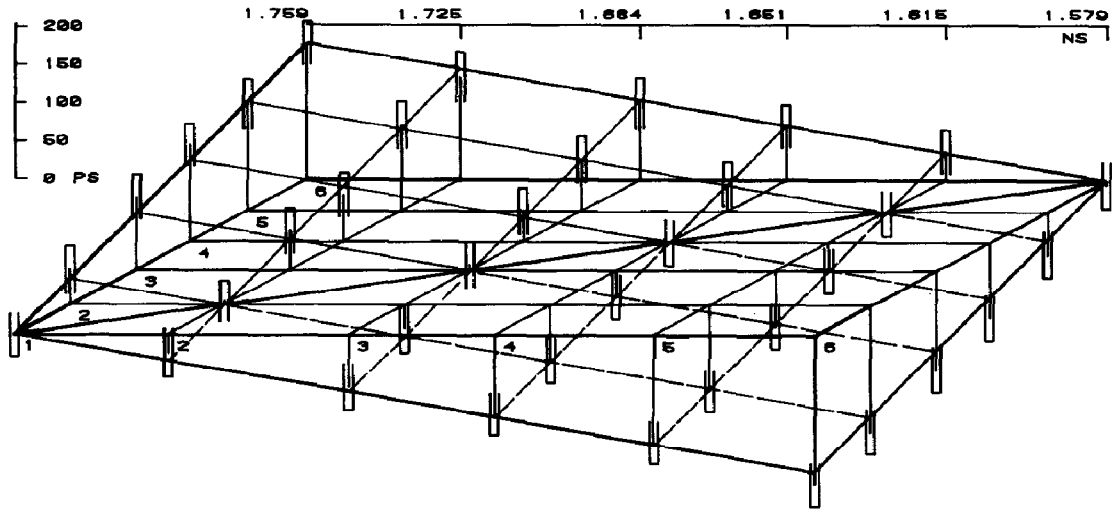

Fig. 6. A chess-board stick plot for type II measurements ($k = 4.32 \times 10^8\,s^{-1}$, $k_q = 3.44 \times 10^9$ l mol^{-1} s^{-1}) (see text).

Comparison of Fig. 2 with Fig. 7 gives the answer to the first question. No obvious distortion can be detected, except that the statistics seem to be slightly more advantageous at small (k, k_q) values in Fig. 7.

The moderate shift of the minimum coordinates is the consequence of the different error distribution and lies well within the tolerable limit. Therefore Fig. 7 can be considered as evidence that our measurement errors are random and that the model applied is consistent with the experimental data.

The second question deals with the dependence of the accuracy of the rate constants on the measurement precision. Computational studies reveal a nearly linear course for type I information, *i.e.* a reduction in $t_{ij} - \tau_{ij}$ by a factor of 2 reduces the uncertainty intervals for k and k_q by a factor of 2.

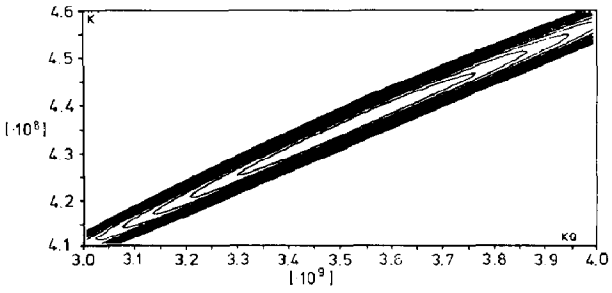

Fig. 7. An IES map of simulated type I measurements: a computer-simulated map analogous to Fig. 2.

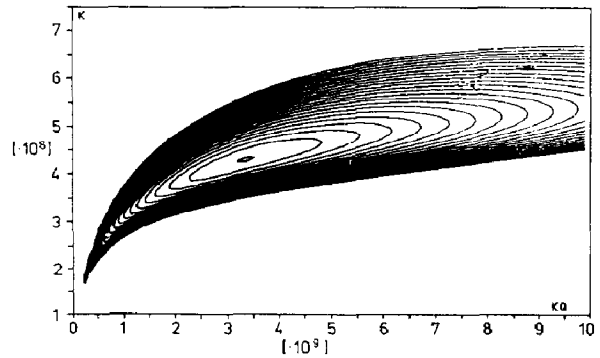

Fig. 8. An IES map for measurements of type C: the error topography for the model case of an extreme concentration span. The distance between the equicontours is 500σ.

For type II information the steepness and the width of the valley decrease significantly to a long groove and hence type II information is not suitable for locating a clean extremum.

The last parameter discussed is the span of the quencher concentrations. Comparison of the contour matrices for type I and type II information shows that an increase in the concentration span favours the determination of the rate constants. This tendency is confirmed in Fig. 8. The experimental conditions are adapted to those of type I information, except for the quencher concentrations which are listed in Table 1. They approximately represent the maximum span which can be realized experimentally.

Further increase in the span leads to more circular shapes in the valley structure and therefore to more accurate rate constants.

5. Conclusions

The dual-beam feature of this experiment turns out to be an important step towards measurements of small changes in relaxation kinetics in the picosecond and nanosecond domain. The time resolution of 20 ps with respect to absolute accuracy was confirmed by the very satisfactory antisym-

metry $\tau_{ij} = -\tau_{ji}$ and the fact that $\tau_{ii} = 0$ is closely approached for all measurements with $i = j$. The absolute data for the rate constants are quite accurate taking into consideration the fact that they originate from relative measurements. It is evident that the method is not restricted to collisional quenching but can be easily adapted to investigate, for example, the influence of temperature, viscosity, solvents, dye concentration or energy transfer.

Acknowledgments

We would like to thank Professor E. Schumacher for critical discussions and encouragement of this work, and W. H. Gerber and J. Baumann for their contribution to some of the calculations. K. O. Marti helped us to survive in the jungle of linking computer systems. This work was financed by the Swiss National Science Foundation (Grant 2.157.78).

References

1 J. B. Birks and I. H. Munro, *Prog. React. Kinet.*, *4* (1967) 239 - 303.
2 G. W. Robinson, J. M. Morris, R. J. Robbins and G. R. Fleming, *J. Mol. Struct.*, *47* (1978) 221 - 235.
J. N. Demas, *J. Chem. Educ.*, *53* (1976) 657 - 663.
D. Rehm and A. Weller, *Isr. J. Chem.*, *8* (1970) 259 - 271.
H. Schomburg, H. Staerk and A. Weller, *Chem. Phys. Lett.*, *21* (1973) 433 - 436.
K. Schulten, H. Staerk, H.-J. Werner and B. Nickel, *Z. Phys. Chem. N.F.*, *101* (1976) 371.
G. Porter and C. J. Tredwell, *Chem. Phys. Lett.*, *56* (1978) 278 - 282.
M. D. Archer, M. I. C. Ferreira, G. Porter and C. J. Tredwell, *Nouv. J. Chim.*, *1* (1977) 9 - 12.
G. Calzaferri, H. Gugger and S. Leutwyler, *Helv. Chim. Acta*, *59* (1976) 1969.
3 D. Rehm and A. Weller, *Ber. Bunsenges. Phys. Chem.*, *73* (1969) 834 - 839.
4 H. Gugger and G. Calzaferri, *J. Photochem.*, *13* (1980) 21 - 33.
5 H. Gugger and G. Calzaferri, *J. Photochem.*, *13* (1980) 295 - 307.
6 P. R. Bevington, *Data Reduction and Error Analysis for the Physical Sciences*, McGraw-Hill, New York, 1969.
7 W. H. Gerber, *FORTRAN Plot Routine CONTOUR*, Institute for Inorganic Chemistry, University of Bern, 1977.